Available online at www.sciencedirect.com
ScienceDirect
Trans. Nonferrous Met. Soc. China 33(2023) 494−506
Transactions of Nonferrous Metals Society of China
www.tnmsc.cn

Surface, mechanical, and in vitro corrosion properties of arc-deposited TiAlN ceramic coating on biomedical Ti6Al4V alloy

Mohamed HUSSEIN[1], Madhan KUMAR[1], Nestor ANKAH[1,2], Ahmed ABDELAAL[2]

1. Interdisciplinary Research Center for Advanced Materials, King Fahd University of Petroleum & Minerals, Dhahran 31261, Saudi Arabia;
2. Department of Mechanical Engineering, King Fahd University of Petroleum & Minerals, Dhahran 31261, Saudi Arabia

Received 14 October 2021; accepted 29 March 2022

Abstract: The surface characteristics and in vitro corrosion properties of nanocrystalline TiAlN coating deposited on biomedical Ti6Al4V alloy by cathodic arc evaporation were studied. The structure and surface morphology were analyzed using XRD and FE-SEM. The surface microhardness was characterized using microindentation. The in vitro corrosion was carried out in simulated body fluid and artificial saliva. The results exhibited that a TiAlN film was deposited with an enhanced surface hardness of 44.4 GPa, a elastic modulus of 419.9 GPa, and enhanced resistance to plastic deformation compared to uncoated alloy. The wetting angle of TiAlN coated surfaces ((86.27±2.2)°) was larger than that of uncoated Ti6Al4V surfaces ((70.61±1.25)°). Biocorrosion examinations revealed that TiAlN-coated Ti6Al4V alloy exhibited a significant positive shift of about 150 mV in corrosion potential with the notable reduction of about one order of magnitude in corrosion current density and higher charge transfer resistance, confirming the improved barrier performance. The surface, mechanical and corrosion performance of TiAlN coating was enhanced compared to uncoated alloy.

Key words: CA-PVD; TiAlN; coating; corrosion; biomedical alloy; titanium

1 Introduction

Three types of metals and alloys: 316 L stainless steels, titanium, and cobalt−chromium alloys, are mainly used for hard tissue replacement, particularly in dental and orthopedic implants. While these materials have high mechanical properties, their biocompatibility and wear are relatively low [1]. Additionally, it has been reported that certain metallic ions (Cr, Co, Ni, and V) formed during in vitro corrosion impair biocompatibility and inhibited immune response as measured by cell proliferation [2]. Magnesium alloys have garnered considerable interest as novel bio-implant materials for short-term implants applications due to their numerous advantages, including high specific strength, excellent biocompatibility, low modulus of elasticity, and biodegradability. However, magnesium and its alloys are very corrosive in the physiological environment, limiting their biomedical applications [3−5]. Compared to SS and Co-based alloys, the Ti-based alloy has been used widely for biomedical uses due to enhanced corrosion properties and biocompatibility [6]. However, the Ti and Ti-based alloys reduced resistance to shear, leading to the release of metal ions, which caused inflammation and reduced the lifetime of the implant materials [6]. Commercial Ti−6Al−4V (Ti64) alloy, with (β+α) microstructure, has been used in implants and dental applications for the past few decades [7]. However, due to the

Corresponding author: Mohamed HUSSEIN, E-mail: mahussein@kfupm.edu.sa, mahussein1980@gmail.com
DOI: 10.1016/S1003-6326(22)66122-3

toxicity of some alloying elements, corrosion and wear products produced by the alloy, for example, the presence of Al and V induced inflammation and toxicity, respectively, affecting the long-term biocompatibility of Ti64 alloy [8]. The reported lifetime of Ti64 alloy in human body fluid is between 12 and 15 years [9], which means that a youthful patient with an artificial joint will require revision surgery. Titanium and its alloys have a higher resistance to corrosion due to the formation of a protective and adherent oxide film composed primarily of TiO_2. On the other hand, this film is unstable in reducing or complexing media; the active behavior of Ti64 alloy in reducing media is due to corrosion of the β phase enriched in V. Vanadium oxides are soluble in acidic solutions [10]. As a result, a variety of surface engineering solutions have been developed to circumvent these constraints. Surface engineering of Ti-based alloys is necessary to enhance their surface characteristics, wear resistance, and corrosion protection [11−13]. The deposited layer should be biocompatible, adhere well to the substrate, and pose higher corrosion resistance in psychological mediums.

Numerous surface treatments and coatings have been applied to enhancing service life and function characteristics, such as corrosion, resistance to wear, and biocompatibilities for biomedical uses [11−14]. For instance, nitriding of the Ti surface is performed to enhance surface hardening. It showed enhanced mechanical, corrosion, and wear properties [15]. TiNbZr and Ti64 biomedical alloys were coated with a TiN layer and the coated samples showed enhanced surface hardness, antibacterial properties, and in vitro corrosion protection in artificial saliva and simulated body fluid [16,17]. TiAlN coating is chemically inert and thermally stable, and hard ceramic coatings improve the corrosion protection of metallic surfaces. TiAlN coating showed enhanced hardness, wear resistance, and erosion resistance than binary TiN coating [18]. TiAlN exhibited improved corrosion resistance compared to Ni−Cr dental casting base metal [7] and the potential to support tissue growth on the surface of dental implants [19]. TiAlN can be deposited using different methods such as chemical vapor deposition, and physical vapor deposition (PVD) [20,21]. Among the different coating processes, the PVD process comparatively performs in relatively low deposition temperature, and a broad range of coating thickness could be deposited. Moreover, the higher temperature of other coating processing may produce along with higher residual stresses [22]. TiAlN coating was reported previously for cutting tools applications [23], investigations of TiAlN coating structure and mechanical properties [24], corrosion studies in HCl medium [24], and cell viability assay [25]. Several studies reported the characteristics of TiAlN deposited coating over Ti64 alloy. The adhesion of TiAlN sputtered coatings was studied [26]. Corrosion studies for TiAlN coating deposited on Ti64 in HCl [24], and in NaCl solution [27], were conducted. Thus, while there are several studies on TiAlN coated Ti64 alloys, there have been few reports on biomedical fields. However, up to the authors' knowledge in this work, none have studied the in vitro corrosion behavior of TiAlN deposited by a cathodic arc (CA-PVD) over Ti64 alloy in simulated body fluid (SBF), and in artificial saliva (AS). Therefore, more investigations are required, such as mechanical and in vitro corrosion in SBF, AS, and wettability study to evaluate the possibility of use of TiAlN coating for biomedical uses.

This work aims to deposit TiAlN ceramic coating by a CA-PVD technique on Ti64 alloy, and to study the effect of TiAlN coating on surface characteristics, wettability and in vitro corrosion properties for possible applications in orthopedic and dental applications. X-ray diffraction technique (XRD) and Raman spectroscopy were utilized to examine the structure of the coating. Scanning electron microscopy (SEM) with energy dispersive X-ray analysis (EDX) was used to analyze the morphology and elemental analysis of the coating. The coatings adhesion was examined using the scratch test. The effectiveness of the synthesized coating was evaluated by studying the mechanical, wettability, and in vitro corrosion performance in different physiological mediums (SBF and AS).

2 Experimental

2.1 TiAlN coating preparation

A commercial Ti64 alloy purchased from Xian Saite Materials Development Co., China, was cuted with a dimension of 25 mm × 25 mm × 3 mm. The samples were ground using 200, 400, 600 and 800 SiC, then polished using a 0.5 μm Al_2O_3 solution,

and then cleaned in acetone ultrasonically. The TiAlN coatings were produced utilizing a Sulzer Cathodic Arc Evaporation (CAE) system (Metaplas, Domino Mini, Germany) [16,17]. The chamber was heated to about 500 °C while rotating the samples before initiating the coating process. The samples were rotated at 2 r/min in a clockwise direction. The surface of the workpiece was cleaned through the Arc Enhanced Glow discharge process (AEGD). A cathode (45Ti−55Al, wt.%) provided by Sulzer (Germany) was used during this process. A shield in front of the AEGD cathode absorbs the positive ions, as a result, excess electrons were produced in the chamber. At this stage, 1 Pa of argon was introduced into the chamber resulting in its ionization by the high-velocity electrons. The positively charged Ar ions are propelled towards the direction of the negatively biased substrates. The accelerated Ar ions impact the surface of the substrate with high energies, resulting in the removal of residual dust, an oxide layer, and other impurities that could be detrimental to the quality of the coating. After AEGD, the coating deposition starts immediately. The evaporator current on the target was 150 A. The total ampere-hour (A·h) of 400 A·h was set. The N_2 gas flow rate was 500 mL/s, and the pressure was 6.5 Pa. The coating duration was 90 min.

2.2 Microstructure and surface characterization

XRD (Rigaku, Kurary, Japan) with Cu K_α radiation with 0.15406 nm wavelength conducted at 40 kV and 30 mA was used to analyze the phases of the coating. 2θ angle was varied between 20° and 90° at a step size of 0.02 and scanning rate of 1.2 (°)/min. Surface morphology was analyzed using SEM (JEOL, Japan). The elemental composition of the coating was analyzed using EDX. Raman spectroscopy optical microscopy (DXR™ 2 Raman Microscope) manufactured by Thermo Fisher Scientific was used to take the Raman spectrum of the coated sample. The laser power of 6 mW and a wavelength of 455 nm with a spot size of 0.6 μm were used.

Surface roughness was characterized using GTK-A, 3D optical profiler from Bruker Co. The wetting characteristics of the samples were examined using contact angle measurement via a sessile drop method using optical contact angle measurement goniometer (DM−501, Kyowa Interface Science Co., Ltd, Japan). At least five readings were taken for each measurement of water (3 μL) contact angle, and then an averaged value was reported for final results.

2.3 Micro-indentation and scratch tests

Microhardness and indentation modulus were evaluated utilizing a microcombi tester (CSM, Switzerland). Vickers indenter (V-H 86) with a diamond tip was utilized for the micro-indentation test. 100 mN indentation load was applied with holding time of 10 s. Five indentations were carried out at 0.5 mm intervals, Oliver & Pharr approach [28] was used to calculate the hardness and modulus.

Scratch resistance performance was carried out using CSM microcombi tester fitted with a Rockwell indenter. The indenter has a diamond stylus tip that is drawn across the surface of the coating with a linear progressing load. The indenter tip radius was 100 μm. The test was performed with a load ranging from 0.03 to 30 N at a loading rate of 0.249 N/s. The scratch length was 10 mm with a scratch speed of 5.5 mm/min. The linear progressing scratch load was applied until spallation, delamination, or failure of the coating. The first critical load (L_{c1}) was defined as the minimum load, at which the first crack or failure event took place and was accurately observed utilizing an inbuilt acoustic emission signal, and was corroborated by scanning electron microscopy (SEM).

2.4 In vitro corrosion studies in simulated body fluid and artificial saliva

Ti-based materials such as Ti−6Al−4V alloy have been widely applied in the field of orthopedic/dental implants. Therefore, the current study uses simulated body fluid (SBF) and artificial saliva (AS) to mimic the medium for orthopedic and dental applications, respectively. In vitro corrosion analysis of the uncoated and coated substrates was done using the Gamry Reference 6000 Potentiostat instrument through three-electrode cell assembly with graphite rod as an auxiliary, saturated calomel as a reference, and the Ti alloy specimens as a working electrode, respectively. The two different physiological mediums such as AS and SBF were produced according to the previous report [12,29] and selected as the testing electrolytes. To reach steady open circuit potential (OCP), the specimens with an

exposure area of 1.76 cm^2 were exposed to the testing electrolytes for 30 min before all the corrosion tests. Electrochemical impedance spectroscopic (EIS) tests were done at OCP using the frequencies region from 10^5 to 10^{-2} Hz with an amplitude of 10 mV. The equivalent circuit investigation of the obtained EIS curves was performed by the inbuilt software, Echem analysis. The potentiodynamic polarization (PDP) experiments were carried out by selecting the applied potential ranging from −250 to 1500 mV at the scan rate of 1.0 mV/s.

3 Results and discussion

3.1 Structure analysis

Figure 1 depicts the XRD patterns for uncoated Ti64 alloy substrate and CA-PVD TiAlN film-coated Ti64 alloy. The coating showed crystallographic planes of (111), (102), (200) and (220) orientation peaks. Compared to the position of the peaks of TiN [16,17], the position of TiAlN peaks is slightly shifted to the higher value of 2θ due to the addition of Al in TiN [30] as a result of contraction of the lattice due to the substitution of Ti with Al, which has a smaller radius of 0.143 nm than that of Ti (0.146 nm). The crystallite size (D) of the TiAlN coating was 22.9 nm as calculated using Scherer equating (D=0.9λ/(βcos θ)) [19], where θ is peak position, and λ is the XRD wavelength.

Raman spectrum is a powerful analytical tool for analyzing the film [30]. The Raman spectra for CA-PVD TiAlN coating is shown in Fig. 2 in the range of 50 to 1500 cm^{-1}. According to the literature [31], the low-wavenumber band of the

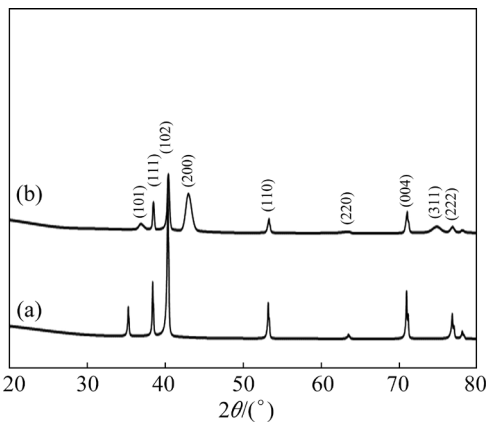

Fig. 1 XRD patterns of bare Ti64 alloy (a) and TiAlN coating (b)

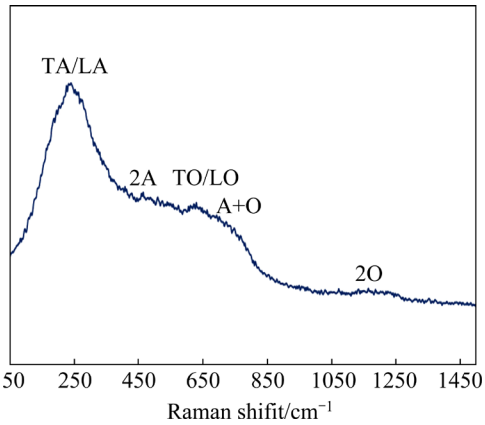

Fig. 2 Raman spectra of TiAlN coating on Ti64 alloy

TiAlN coating corresponds to the TA and LA modes, the mid-wavenumber band to the 2A, TO/LO, and A+O modes, and the high-wavenumber band to the 2O modes. The Raman spectrum of Ti−Al−N coatings is dominated by the vibrations of the heavy metal ions (usually 150−350 cm^{-1}) and, in the optical range, by the vibrations of the lighter N ions (typically 400−650 cm^{-1}) [32]. The Ti ions are responsible for dispersion in the acoustic range, while nitrogen ions are responsible for the dispersion of the optical range [33]. Two wide bands were visible in the spectra, focused on 240 and 628 cm^{-1}. These bands are caused by first-order transverse acoustics in the 150−350 cm^{-1} range (LA and TA) and optical modes in the 400−650 cm^{-1} range (LO and TO) [34]. Additionally, the second-order acoustic (2A) was detected at 466 cm^{-1}. Higher frequency spectral density is subsequently generated by second-order transitions (A+O, 2O). The obtained Raman result is agreed with a previous report for TiAlN deposited coating onto CP−Ti substrates [6] and steel substrate [35], respectively.

The surface morphologies of CA-PVD TiAlN coating and Ti64 substrates are presented in Fig. 3. It showed the incorporation of microparticles that resulted in surface irregularity [36]. These macro-particles are a distinctive feature of cathodic arc process and are made of unreacted cathode material. The sizes are dependent on deposition parameters and the cathode used [37]. These droplets are deleterious to coating quality and performance. The previous studies showed that these defects are 1−40 μm. From Figs. 3(a, b), the majority of surface defects in these coatings are less than 1 μm in diameter, indicating a significant particle size

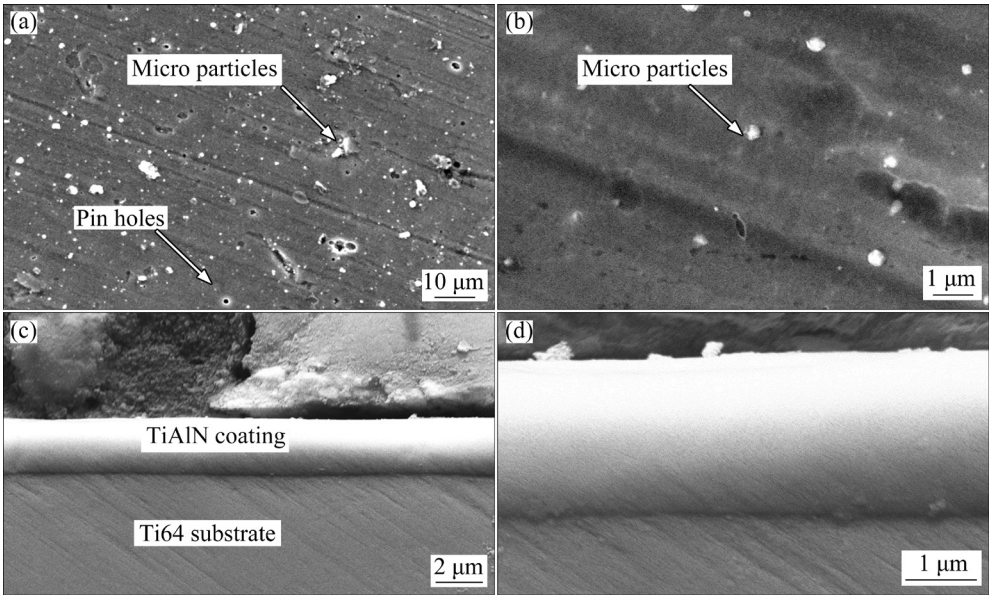

Fig. 3 SEM images of TiAlN coating: (a, b) Surface micrograph; (c, d) Cross section

reduction, which confirms the effective coating obtained as characteristics of the high plasma density of CA-PVD. This is due to the cathodic arc PVD process's characteristic of high plasma density, which enables effective and efficient deposition of dense coatings with a minimum of microparticles. The cross-sectional SEM images of coatings are shown in Figs. 3(c, d). It demonstrates the coatings' uniformity, the thickness of 2.6 μm. Additionally, the cross-sections demonstrate that the coatings are continuous and free of internal macro defects. EDX spectra (Fig. S1) reveal the content of Ti (47.2±4) wt.%, Al (27.8 wt.%) and N (25±1) wt.%, respectively.

3.2 Mechanical and surface characteristics

Loading and unloading curves for Ti64 alloy and TiAlN coating are depicted in Fig. 4. The measured microhardness (H), indentation modulus (E), and calculated H^3/E^2 ratio for the coating and bare substrate are depicted in Table 1. The result exhibited an increase in the microhardness of the TiAlN coating substrate ((44.47±2.42) GPa), five times compared to the uncoated substrate. The hardness is significantly influenced by the stress level and microstructure of the coating. H^3/E^2 was used to assess the resistance of thin films to plastic deformation [16]. The modulus of elasticity was extracted from the unloading part of the load−displacement curve shown in Fig. 4, using Oliver and Pharr approach, and the modulus was also increased from 176.5 to 419.9 GPa (Table 1). This was a result of the increased bond strength of TiAlN coating. From indentation test results, H^3/E^2 was calculated and it was increased for TiAlN coating (0.46 GPa) compared to (0.0128 GPa) of the uncoated Ti64 substrate, which may contribute to

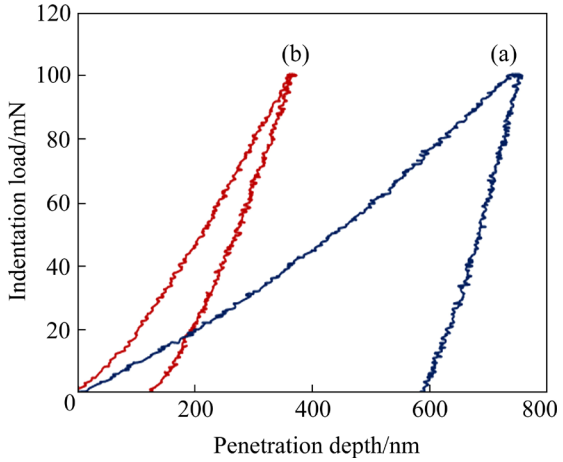

Fig. 4 Load−displacement curves of loading and unloading samples: (a) Ti64 alloy; (b) TiAlN coating

Table 1 Microhardness, indentation modulus, and surface roughness of coated and uncoated alloy

Sample	Hardness, H/GPa	Modulus, E/GPa	(H^3/E^2)/GPa	R_a/nm
Ti64 alloy	7.55 ±1.3	176.5±12	0.0138	89
TiAlN coating	44.47 ±2.42	419.9±30.1	0.49	161

reducing wear rate due to enhanced resistance to plastic deformation [16]. The hardness to modulus ratio, also known as the elastic strain to failure ratio (*H*/*E* ratio), is a typical value used to determine the toughness and resistance to deformation. The *H*/*E* ratio of TiAlN coating was greater than that of the substrates. A high *H*/*E* value, according to LEYLAND and MATTHEWS, indicates a high level of wear resistance [35]. Therefore, enhancement of the surface hardness by applying TiAlN coating will contribute to improvement in the wear resistance and hence minimize the creation of the wear debris, enhancing the implants' lifetime [5]. The coating's high hardness can be attributed to solid solution strengthening caused by densification of grain boundaries, resulting in the nanocrystalline structure of coating [38]. The crystallite size of the TiAlN coating is 22.9 nm according to the Scherer formula. Also, due to the presence of hard nitride phases, the coating layers have higher hardness than the substrate [39]. The hard coating obviously will contribute to increasing the wear resistance [5].

The surface roughness measurement reveals that the roughness amplitude (R_a) for coated samples (R_a=161 nm) is rougher than the uncoated polished Ti64 sample (R_a=89 nm) (Fig. 5(a)) as depicted in the 3D profilometer (Fig. 5). The higher roughness of the coating is associated with the distinctive pits and microparticles and observed in the coating synthesized by CA-PVD. According to Ref. [40], metal surfaces with a low microscale to nanophase morphology promote osteoblast adhesion. The microtopographic pattern maximizes the interaction of mineralized bone with the implant surface [41]. Therefore, the synthesized TiAlN coating, 160 nm would contribute to enhancing the interaction with the implant. The primary disadvantage of CA-PVD is the formation of macro droplets during deposition, which results in rougher morphology of the films [42]. The increased roughness of the coating is frequently attributed to macroparticles formed as a result of the increased number of droplets emitted by the low melting Al element. DING et al [43] reported that increasing the Al content of CA PVD coatings increases their roughness. CYSTER et al [44] demonstrated the critical role of topology and surface chemistry in cell-substrate interactions. GUÈHENNEC et al [45] reported that rough surfaces promote biochemical

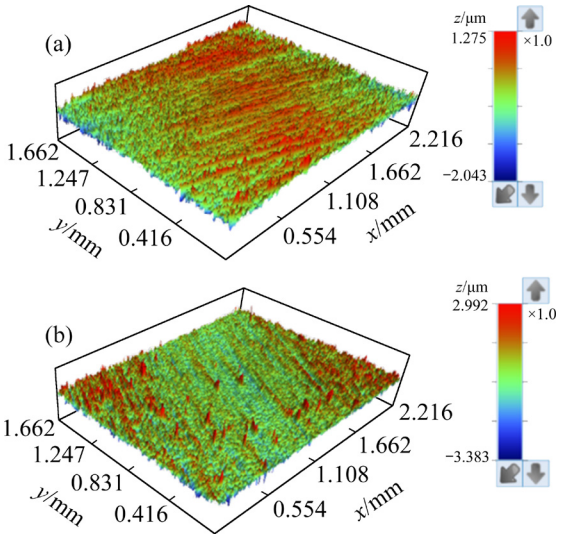

Fig. 5 3D profilometer for T64 alloy (a) and TiAlN coating (b)

stability. Rough surface and high surface energy promoted cell attachment and proliferation [25,46]. Along with the topography of the surface, the wettability of the surface can influence cellular behavior. The wettability of a surface is critical for protein absorption, cell attachment, and spread [47]. The contact angles of deionized water drop on the surface were evaluated on the coated and uncoated alloys. Figure 6 presents the water contact angle for the uncoated and coated sample with their images. The wetting angle of TiAlN coated surfaces measured in this study ((86.27±2.2))°) was greater than that of the uncoated Ti64 surface ((70.61±1.25)°).

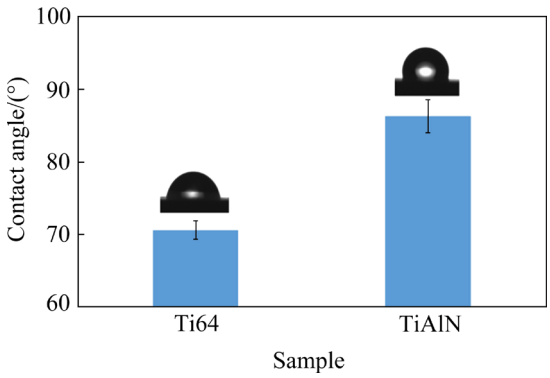

Fig. 6 Contact angle for Ti64 alloy and TiAlN coating

3.3 Scratch test analysis

During scratch, there is a continuous elastoplastic deformation of the coating until eventual failure. To distinctively identify a failure event when there is no clear spallation or

delamination, the concept of the critical load was employed where the minimum load at which the first failure event took place is referred to the first critical load of the coating. At the critical load, there is a well-defined failure event typified by an acute increase in the acoustic emission signal as presented in Fig. S2, with the panoramic view of the whole scratch track. As shown in Fig. S2 for TiAlN, a signal spike in acoustic emission was observed at a load of 13.5 N. Typically, two fundamental modes of failure are experienced in the process of scratching, namely, cohesive and adhesive failure. In cohesive failure there are significant chippings at the edges of the scratch track with no delamination or spallation of the coating, whereas, adhesive failure is characterized by severe delamination and spallation. Failure during scratch is a complex process such that a combination of both failure modes usually takes place. The critical load can significantly be affected by factors such as the hardness of the coating, interface properties of the coating and substrate, the loading rate, scratch speed indenter type as well as instrument compliance [48]. Figure 7 shows SEM images along the scratch track. It can be observed in Fig. 7(a) that there were significant ploughing and continuous plastic deformation of the substrate as the stylus moved across the coating surface, while in Fig. 7(b), cracks were observed both within and along the edges of the scratch track. The predominant failure mechanism observed in the TiAlN coating was tensile cracks as a result of elevated tensile stresses behind the indenter [49]. This failure type is typically distinguished by semicircular cracks in the scratch direction. The contact stress at L_{c1} was obtained according to the equation, $PC=L_{c1}/A$, where A is the contact area between the indenter and the coating surface, estimated from the width of the scratch (Fig. 7(b)). The estimated contact stress calculated according to Ref. [50] at failure is 3.7 GPa, which is about 24 times the peak contact stress experienced by the human hip (for 200 mm cup radius and 100 μm radial clearance) [51]. Therefore, TiAlN coating deposited with cathodic arc evaporation will boost the lifespan of the implant.

3.4 In vitro corrosion analysis in SBF and AS

Two different physiologic mediums such as SBF and AS were selected to assess the in vitro corrosion-resistant performance of coated Ti64 alloy for its application in orthopedic and dental applications. Figure 8 displays the representative PDP curves of the uncoated and coated Ti64 alloy substrates in SBF and AS medium. No distinct variation is obtained in the cathodic branches of the PDP curves, revealing that oxygen reduction is the major cathodic reaction in all the substrates. However, the anodic branches of the PDP curves exhibited significant variation in the tested potential regions.

In the initial stage of anodic polarization, bare alloy presented a steep anodic slope up to 300 mV in both tested mediums, representing the metal dissolution on the Ti64 alloy surface. In addition, the slope of the anodic branch is almost vertical, with a slight slope above 400 mV and it continued to be the same till the end. This observation is possibly ascribed to less oxygen diffusion owing to the existence of passivation film on the Ti64 alloy substrate [52]. In contrast, the anodic slope of coated Ti64 alloy is found to be comparatively reduced steep, indicating the reduction in anodic dissolution. Besides, contrasting to the bare alloy, it displays a significant reduction in current density in the anodic polarization area from initial almost to

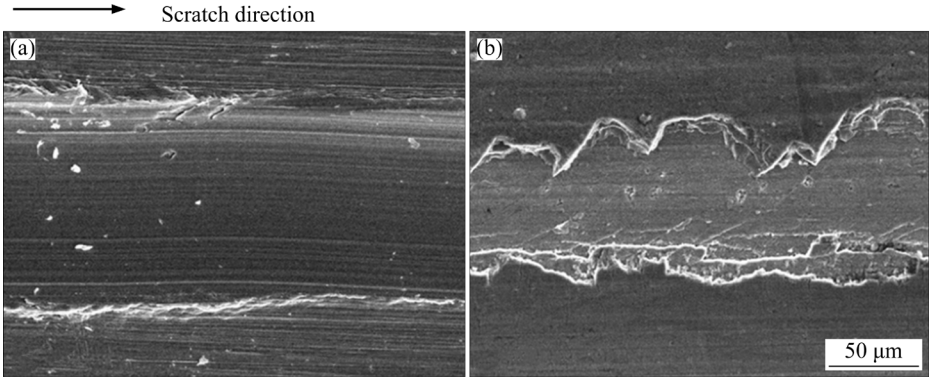

Fig. 7 SEM images of scratch track for Ti64 alloy (a) and TiAlN coating (b)

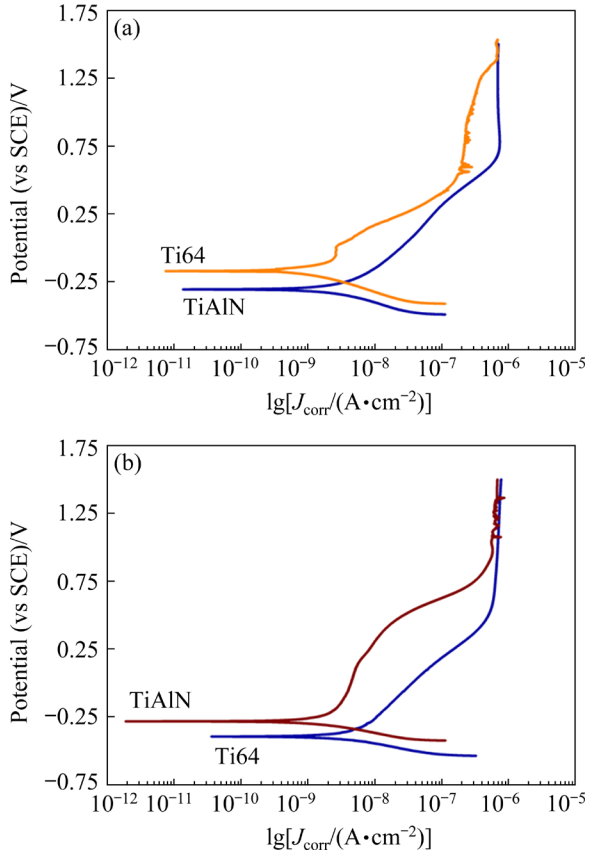

Fig. 8 PDP plots of uncoated Ti64 and TiAlN coating in AS (a) and SBF (b) medium

end. Thus, these interpretations validated that coated Ti64 displayed improved corrosion-resistant performance in both mediums in comparison with the bare. The coated Ti64 alloy exhibited nobler shirt in φ_{corr} values in both SBF and AS medium compared to that of bare, revealing the improved corrosion-resistant performance, which is attributed to the effective barrier features of the TiAlN layer that is more efficient than the naturally formed passivation film on the Ti64 substrate [17]. Bare substrate showed a distinct passivation characteristic above 400 mV; however, the TiAlN coated substrate did not exhibit a noticeable passivation plateau, though it is shown less current densities on the anodic branch in the investigated potential region. The resultant values including corrosion current density (J_{corr}), corrosion potential (φ_{corr}), anodic as well as cathodic Tafel slopes (β_a and β_c) are displayed in Table 2. In general, φ_{corr} infers only qualitative analysis concerning the proneness to metallic dissolution, whereas J_{corr} provides quantitative information regarding the precise degrees of the corrosion rate. Thus, the corrosion current describes the protection magnitude of the passive film on the metallic surface, and a low corrosion current density generally reveals an improved corrosion resistance. J_{corr} is a parameter extracted by the resultant of the two curves, demonstrating the phenomena of anodic oxidation and cathodic reduction which occur concurrently in the vicinity of φ_{corr}. Generally, higher φ_{corr} and lower J_{corr} values signify that the metallic substrate exhibits comparatively improved corrosion resistance [8]. From Table 2, it is clear that the J_{corr} values are higher in the case of the bare Ti64 alloy in both SBF and AS medium. Ti−6Al−4V is α+β titanium alloy. The variation in elemental configuration and electrochemical activity between the α and β phases prompts a galvanic effect and reduces the corrosion resistance [53]. METIKOŠ-HUKOVIĆ et al [54] reported that the formation and dispersion of vacancies in the passive film, and adsorption of Cl^- ions in such vacancies, reduce the stability of the oxide film and increase the proneness of the Ti64 alloy to corrosion. Comparing the J_{corr} values of uncoated substrates, coated-Ti alloy substrates exhibited pointedly lower values in both tested media. The lower J_{corr} values implied that the existence of the TiAlN layer improved the corrosion protection performance of the Ti64 alloy surface in the simulated biological media. To validate the quality of Tafel fit analysis, chi-squared values (χ^2) are monitored and summarized in Table 2. Moreover, the passivation current density (J_{pass}) of

Table 2 PDP parameters for uncoated and TiAlN coating in SBF and AS media

Sample	φ_{corr}(vs SCE)/mV	J_{corr}/ (10^{-2} μA·cm^2)	β_a/ (mV·dec^{-1})	β_b/ (mV·dec^{-1})	$\chi^2/10^{-3}$	Corrosion rate/ (μm·year^{-1})
Ti64 alloy in SBF	−391	59.740	93	79	88.25	2.984
TiAlN coating in SBF	−268	12.321	88	95	37.54	0.6153
Ti64 alloy in AS	−339	57.232	77	92	77.47	2.858
TiAlN coating in AS	−192	2.135	98	84	56.87	0.106

TiAlN-coated Ti substrate was lower as compared to the uncoated samples, while the J_{pass} value of the TiAlN samples was lower than that in the saliva medium. The decreased J_{pass} and J_{corr} values corroborated that the existence of the PVD-processed TiAlN layer improved the surface protective performance of the Ti64 alloy surface against corrosion in the physiological media. It has already been reported that the corrosion protection of Ti alloys in physiological media could be improved using TiAlN films [55].

Characteristic EIS curves of the uncoated and coated substrate are displayed in Figs. 9 and 10 in Nyquist and Bode formats. The recorded and the simulated EIS data are symbolized by solid symbols and complete lines, respectively. The obtained EIS curves assessed the nature of electrochemical interactions between TiAlN coating and physiological media and offered prominent information about the corrosion of Ti alloy in the physiological mediums. The Nyquist plot in Fig. 10 exhibits distinguishing capacitance characteristics in the investigated high-, medium-, and low-frequency, which is signified by an incomplete capacitor arc. This further revealed that the electrochemical reaction of the substrates is controlled through the charge transfer happening at the metal/solution interface. All the Nyquist plots (Figs. 10(a, b)) exhibited the distorted capacitive resistance arcs and the coated substrate in both SBF and AS media exhibited a larger diameter of capacitive arc, representing an improved corrosion resistance compared to that of the uncoated substrate [29]. In general, the semi-circle shape of the Nyquist plot is directly governed by factors including frequency dispersion, porosity, and surface heterogeneity of the materials under investigation [56]. The enhanced corrosion protection behavior was similarly revealed by a significant increase in total impedance values ($|Z|$) indicated in the Bode plot (Figs. 9(a, b)). Comparing the $|Z|$ values of coated substrates in SBF and AS media, it was possible to observe that the coated substrate in SBF was slightly higher than

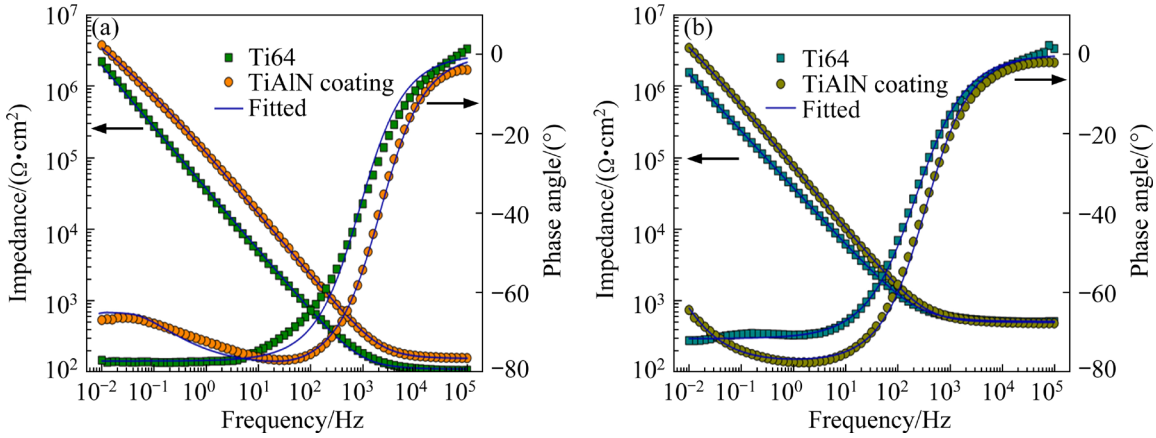

Fig. 9 Bode plots of uncoated and TiAlN coating in SBF (a) and AS (b) media

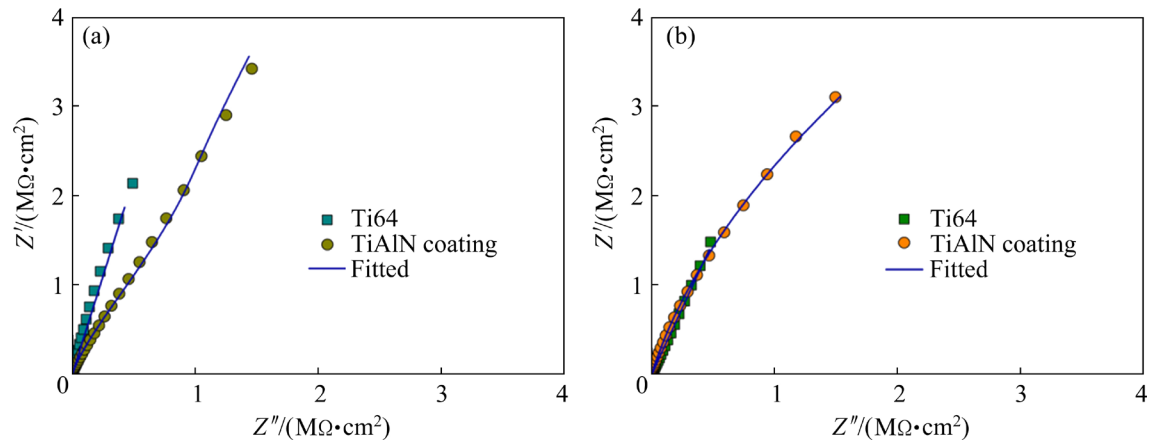

Fig. 10 Nyquist plots of uncoated and TiAlN coating in SBF (a) and AS (b) media

that in AS medium. In the Bode graph, the impedance value in the higher frequencies is nearly constant, and the phase angle is close to 0°, representing the resistive behavior of the tested solution between the reference and working electrodes. Then, the impedance response is shown linear behavior and the phase angle is found to be close to 80° in the mid- and low-frequency regions, accompanying the capacitive response features of the protective coating are more effective [57]. From Fig. 9, the coated substrate exhibited a high phase angle (>80°) in the wide region of 10^{-2}–10^{2} Hz, suggesting the quasi-ideal capacitive behavior of TiAlN coatings effectively obstructs the permeation of aggressive species into the coating, inhibiting the corrosive damage of the Ti64 alloy substrate. Moreover, the phase angle of the coated substrate in SBF was slightly higher than that of coated substrates in AS medium, representing that the protective/capacitive response of TiAlN coating is slightly higher in SBF medium. To achieve more quantitative insights on the biocorrosion resistant behavior of the TiAlN coatings on Ti64 alloy substrates, an equivalent circuit (EC) models, R_s[CPE$_{dl}$$R_{ct}$], for the bare substrate (Fig. 11) and an additional EC, R_s(CPE$_f$[R_f(CPE$_{dl}$$R_{ct}$)]), for the coated substrates were employed (Fig. 11) for EIS simulation investigations [58,59]. The R_s, R_f, and R_{ct} represent the electrolytic, coating and charge transfer resistances, respectively. CPE$_{dl}$ and CPE$_f$ signify the constants-phase element for the double layer and coating, respectively. The low-frequency time constant (CPE$_{dl}$ and R_{ct}) reveals the substrate/coating interface, while the CPE$_f$ and R_f denote the high-frequency time constant accompanied by the coating/electrolytic interface. The following empirical equation denotes impedance (Z) of CPE, $Z_{CPE}=Q^{-1}(j\omega)^{-n}$, where Q represents the CPE constant, j defines the imaginary number, angular frequency $\omega=2\pi f$ rad·s^{-1}, and n represents the CPE exponent [60]. In general, the n value is ranging from −1 to +1, in which n=1 designates a pure capacitor, 0 represents a pure resistor, and −1 represents an inductor. All the chi squared (χ^2) value concerning the fitting errors was found to be in the range of 10^{-4}–10^{-3}, signifying the good agreement between the measured and fitted results.

From Table 3, the coated substrates in SBF and AS medium exhibited higher values of R_{ct}, compared with the bare substrate, revealing the enhanced barrier property provided by homogeneous and compact TiAlN film. Particularly, coated Ti64 substrate displayed good barrier performance in SBF, with a film resistance R_f of 37 kΩ·cm^2 and a highest R_{ct} of 4027 kΩ·cm^2 (versus 2064 kΩ·cm^2 for bare). Furthermore, the coated Ti64 alloy presented a significant reduction in the values of CPE$_{dl}$ by two orders of magnitude, validating the substantial decrease in the permeation of violent ions from the tested medium. Therefore, the important advantage of coated Ti64 alloy compared to that of bare alloys in terms of in vitro corrosion resistant performance is revealed in the large capacitive arcs and high R_{ct} with low CPEdl values and nobler φ_{corr} with lower J_{corr} values, thus corroborating the effectiveness and stability of the compact TiAlN film in enhancing the in vitro corrosion resistance of Ti64 alloy substrates in tested physiological mediums.

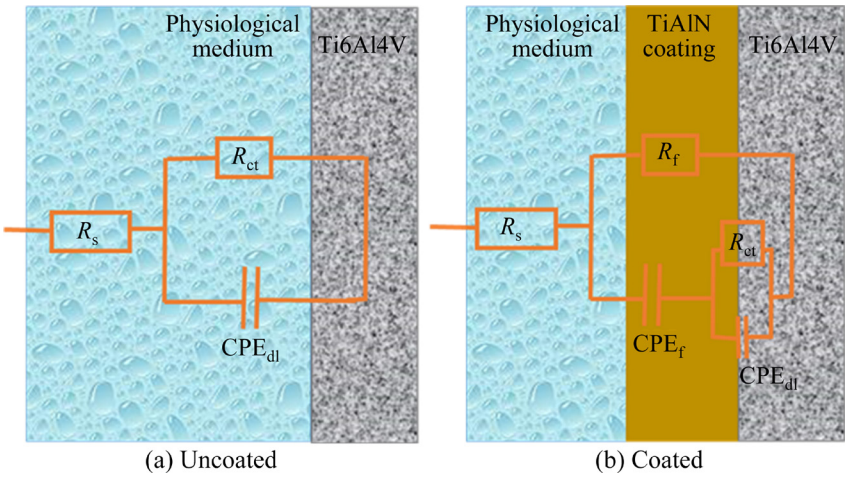

(a) Uncoated (b) Coated

Fig. 11 Equivalent circuit models of uncoated Ti6Al4V (a) and TiAlN coating (b)

Table 3 EIS parameters for uncoated and TiAlN coating in SBF and AS media

Sample	R_s/(Ω·cm^2)	R_{ct}/(kΩ·cm^2)	Q_{dl}/(μF·cm^{-2})	n_{dl}	R_f/(kΩ·cm^2)	Q_f/(μF·cm^{-2})	n_f
Ti64 alloy in SBF	126	2064.412	15.651	0.98	−	−	−
TiAlN coating in SBF	153	4027.275	0.012	0.99	37.753	0.567	0.98
Ti64 alloy in AS	168	1569.027	21.97	0.97	−	−	−
TiAlN coating in AS	172	3523.098	0.045	0.98	34.453	0.634	0.97

4 Conclusions

(1) The microhardness of the arc-deposited TiAlN ceramic coating was five times that of the uncoated Ti64 alloy.

(2) The critical load of the coating was observed to be about 13.5 N. There was no spallation or delamination of the coating during the scratch test indicating well adhesion to the substrate.

(3) The coated layer showed higher resistance to plastic deformation compared to the uncoated Ti64 alloy

(4) In vitro corrosion protection in SBF and AS medium validated the improved surface protective behavior of TiAlN coating compared to uncoated Ti64 alloy against corrosion in simulated body fluid and artificial saliva.

Supplementary materials

The supplementary materials in this paper can be found at: http://tnmsc.csu.edu.cn/download/12-p0494-2021-1340-Supplementary_materials.pdf.

Acknowledgments

The authors would like to acknowledge King Fahd University of Petroleum & Minerals for the provided support.

References

[1] HANAWA T. Biofunctionalization of titanium for dental implant [J]. Japanese Dental Science Review, 2010, 46(2): 93−101.

[2] VLADESCU A, SURMENEVA M A, COTRUT C M, SURMENEV R A, ANTONIAC I V. Bioceramic coatings for metallic implants [M]//Handbook of Bioceramics and Biocomposites. Cham: Springer International Publishing, 2016: 703−733.

[3] CAO G Q, WANG L J, FU Z Y, HU J H, GUAN S K, ZHANG C L, WANG L G, ZHU S J. Chemically anchoring of TiO_2 coating on OH-terminated $Mg_3(PO_3)_2$ surface and its influence on the in vitro degradation resistance of Mg−Zn−Ca alloy [J]. Applied Surface Science, 2014, 308: 38−42.

[4] AMIRNEJAD M, RAJABI M, MOTAVALLI A. Effect of addition of Si on microstructure, mechanical properties, bio-corrosion and cytotoxicity of Mg−6Al−1Zn alloy [J]. Transactions of Nonferrous Metals Society of China, 2018, 28: 1755−1762.

[5] ALI M, HUSSEIN M A, AL-AQEELI N. Magnesium-based composites and alloys for medical applications: A review of mechanical and corrosion properties [J]. Journal of Alloys and Compounds, 2019, 792: 1162−1190.

[6] HUSSEIN M, MOHAMMED A, AL-AQEELI N. Wear characteristics of metallic biomaterials: A review [J]. Materials, 2015, 8: 2749−2768.

[7] SUBRAMANIAN B, MURALEEDHARAN C V, ANANTHAKUMAR R, JAYACHANDRAN M. A comparative study of titanium nitride (TiN), titanium oxy nitride (TiON), and titanium aluminum nitride (TiAlN), as surface coatings for bio implants [J]. Surface and Coatings Technology, 2011, 205: 5014−5020.

[8] HUSSEIN M, ADESINA A Y, KUMAR M, AZEEM M, SOROUR A, AL-AQEELI N. Improvement of in vitro corrosion, wear, and mechanical properties of newly developed Ti alloy by thermal treatment for dental applications [J]. Transactions of Nonferrous Metals Society of China, 2021, 31: 952−966.

[9] RACK H J, QAZI J I. Titanium alloys for biomedical applications [J]. Materials Science and Engineering C, 2006, 26: 1269−1277.

[10] OLIVEIRA M C V, AGUIAR C, VAZQUEZ A M, ROBIN A, BARBOZA M J R. Improving corrosion resistance of Ti−6Al−4V alloy through plasma-assisted PVD deposited nitride coatings [J]. Corrosion Science, 2014, 88: 317−327.

[11] KONG D J, LONG D, WU Y Z, ZHOU C Z. Mechanical properties of hydroxyapatite-zirconia coatings prepared by magnetron sputtering [J]. Transactions of Nonferrous Metals Society of China, 2012, 22: 104−110.

[12] HUSSEIN M A, KUMAR A M, YILBAS B S, AL-AQEELI N. Laser nitriding of the newly developed Ti−20Nb−13Zr at.% biomaterial alloy to enhance its mechanical and corrosion properties in simulated body fluid [J]. Journal of Materials Engineering and Performance, 2017, 26: 5553−5562.

[13] MADHAN KUMAR A, ADESINA A Y, HUSSEIN M A, RAMAKRISHNA S, AL-AQEELI N, AKHTAR S, SARAVANAN S. PEDOT/ FHA nanocomposite coatings on newly developed Ti−Nb−Zr implants: Biocompatibility and surface protection against corrosion and bacterial infections [J]. Materials Science and Engineering C, 2019, 98: 482−495.

[14] YANG X, WANG W L, MA W J, WANG Y, YANG J G, LIU S F, TANG H P. Corrosion and wear properties of micro-arc

oxidation treated Ti6Al4V alloy prepared by selective electron beam melting. [J]. Transactions of Nonferrous Metals Society of China, 2020, 30(8): 2132−2142.

[15] HELSEN J A, BREME H J. Metals as biomaterials [M]. Chichester: Wiley, 1998.

[16] HUSSEIN M A, ANKAH N K, KUMAR A M, AZEEM M A, SARAVANAN S, SOROUR A A, AL AQEELI N. Mechanical, biocorrosion, and antibacterial properties of nanocrystalline TiN coating for orthopedic applications [J]. Ceramics International, 2020, 46: 18573−18583.

[17] HUSSEIN M A, ADESINA Y, KUMAR A M, SOROUR A A, ANKAH N, AL-AQEELI N. Mechanical, in-vitro corrosion, and tribological characteristics of TiN coating produced by cathodic arc physical vapor deposition on Ti20Nb13Zr alloy for biomedical applications [J]. Thin Solid Films, 2020, 709: 138183.

[18] YANG Q, SEO D Y, ZHAO L R, ZENG X J. Erosion resistance performance of magnetron sputtering deposited TiAlN coatings [J]. Surface and Coatings Technology, 2004, 188/189: 168−173.

[19] CHIEN C C, LIU K T, DUH J G, CHANG K W, CHUNG K H. Effect of nitride film coatings on cell compatibility [J]. Dental Materials, 2008, 24: 986−993.

[20] DU L Y, WANG S Q, DU Y, QIU L C, CHEN Z, CHEN X M, LIU Z K, ZHANG C. Deposition of CVD-TiCN and TiAlN coatings guided with thermodynamic calculations. [J]. International Journal of Materials Research, 2018, 109: 277−283.

[21] BOING D, de OLIVEIRA A J, SCHROETER R B. Limiting conditions for application of PVD (TiAlN) and CVD (TiCN/Al_2O_3/TiN) coated cemented carbide grades in the turning of hardened steels [J]. Wear, 2018, 416/417: 54−61.

[22] SHAH A, IZMAN S, ABDUL-KADIR M R, MAS-AYU H. Influence of substrate temperature on adhesion strength of TiN coating of biomedical Ti−13Zr−13Nb alloy [J]. Arabian Journal for Science and Engineering, 2017, 42: 4737−4742.

[23] KUMAR T, PRABU S, GEETHA M, PADMANABHAN K. Comparison of TiAlN, AlCrN, and AlCrN/TiAlN coatings for cutting-tool applications [J]. International Journal of Minerals, Metallurgy and Materials, 2014, 21: 796−805.

[24] TAGHAVI POURIAN AZAR G, ER D L, ÜRGEN M. The role of superimposing pulse bias voltage on DC bias on the macroparticle attachment and structure of TiAlN coatings produced with CA-PVD [J]. Surface and Coatings Technology, 2018, 350: 1050−1057.

[25] JANG H, LEE H, HA J, KIM K, KWON T. Surface characteristics and osteoblast cell response on TiN-and TiAlN-coated Ti implant. [J]. Biomedical Engineering Letters, 2011, 1: 99−107.

[26] DEVIA D M, RESTREPO-PARRA E, ARANGO P J, TSCHIPTSCHIN A P, VELEZ J M. TiAlN coatings deposited by triode magnetron sputtering varying the bias voltage [J]. Applied Surface Science, 2011, 257: 6181−6185.

[27] OLIVEIRA V M C A, VAZQUEZ A M, AGUIAR C, ROBIN A, BARBOZA M J R. Protective effect of plasma-assisted PVD deposited coatings on Ti−6Al−4V alloy in NaCl solutions [J]. Materials & Design, 2015, 88: 1334−1341.

[28] OLIVER W C, PHARR G M. An improved technique for determining hardness and elastic modulus using load and displacement sensing indentation experiments [J]. Journal of Materials Research, 1992, 7: 1564−1583.

[29] HUSSEIN M A, YILBAS B, KUMAR A, DREW R, AL-AQEELI N. Influence of laser nitriding on the surface and corrosion properties of Ti−20Nb−13Zr alloy in artificial saliva for dental applications [J]. Journal of Materials Engineering and Performance, 2018, 27: 4655−4664.

[30] SHUM P W, ZHOU Z F, LI K Y. Optimisation of carbon implantation pre-treatments on the adhesion strength of amorphous carbon coatings on AISI 440C steel substrates [J]. Surface and Coatings Technology, 2003, 166: 213−220.

[31] CONSTABLE C P, YARWOOD J, MÜNZ W D. Raman microscopic studies of PVD hard coatings [J]. Surface and Coatings Technology, 1999, 116/117/118/119: 155−159.

[32] SHULEPOV I, KASHKAROV E, STEPANOV I, SYRTANOV M, SUTYGINA A, SHANENKOV I, OBROSOV A, WEIß S. The formation of composite Ti−Al−N coatings using filtered vacuum arc deposition with separate cathodes [J]. Metals, 2017, 7: 497.

[33] BEJARANO G, ECHAVARRÍA A, QUIRAMA A, OSORIO J. Deposition and property characterization of TaN coatings deposited with different nitrogen contents [J]. Revista EIA, 2016, 25: 69−80.

[34] IPAZ L, APERADOR W, CAICEDO J, ESTEVE J, ZAMBRANO G. A practical application of X-ray spectroscopy in Ti−Al−N and Cr−Al−N thin films [M]// X-ray Spectroscopy, 2012.

[35] LEYLAND A, MATTHEWS A. On the significance of the H/E ratio in wear control: A nanocomposite coating approach to optimised tribological behaviour [J]. Wear, 2000, 246: 1−11.

[36] HARLIN P, BEXELL U, OLSSON M. Influence of surface topography of arc-deposited TiN and sputter-deposited WC/C coatings on the initial material transfer tendency and friction characteristics under dry sliding contact conditions [J]. Surface and Coatings Technology, 2009, 203:1748–1755.

[37] AHARONOV R R, CHHOWALLA M, DHAR S, FONTANA R P, Factors affecting growth defect formation in cathodic arc evaporated coatings [J]. Surface and Coatings Technology, 1996, 82: 334−343.

[38] ZHANG S, WANG H L, ONG S E, SUN D E, LAM BUI X. Hard yet tough nanocomposite coatings–Present status and future trends [J]. Plasma Processes and Polymers, 2007, 4: 219−228.

[39] PALDEY S, DEEVI S C. Single layer and multilayer wear resistant coatings of (Ti, Al)N: A review [J]. Materials Science and Engineering: A, 2003, 342: 58−79.

[40] LIU X Y, CHU P K, DING C X. Surface nano-functionalization of biomaterials [J]. Materials Science and Engineering: R: Reports, 2010, 70: 275−302.

[41] WENNERBERG A, HALLGREN C, JOHANSSON C, DANELLI S. A histomorphometric evaluation of screw-shaped implants each prepared with two surface roughnesses [J]. Clinical Oral Implants Research, 1998, 9: 11−19.

[42] ALI M, HAMZAH E, ABBAS T, HJ MOHD TOFF M R, QAZI I A. Macrodroplet reduction and growth mechanisms in cathodic arc physical vapor deposition of TiN films [J]. Surface Review and Letters, 2008, 15: 653−659.

[43] DING X Z, TAN A L K, ZENG X T, WANG C, YUE T, SUN C Q. Corrosion of CrAlN and TiAlN coatings deposited by lateral rotating cathode arc [J]. Thin Solid Films, 2008, 516: 5716−5720.

[44] CYSTER L A, PARKER K G, PARKER T L, GRANT D M. The effect of surface chemistry and nanotopography of

titanium nitride (TiN) films on 3T3-L1 fibroblasts [J]. Journal of Biomedical Materials Research, 2003, 67A: 138−147.
[45] GUÉHENNEC L, SOUEIDAN A, LAYROLLE P, AMOURIQ Y. Surface treatments of titanium dental implants for rapid osseointegration [J]. Dental Materials, 2007, 23: 844−854.
[46] MAJHY B, PRIYADARSHINI P, SEN A. Effect of surface energy and roughness on cell adhesion and growth–facile surface modification for enhanced cell culture [J]. RSC Advances, 2021, 25: 15467−15476.
[47] KAWAHARA H. Cellular responses to implant materials: biological, physical and chemical factors [J]. International Dental Journal, 1983, 33: 350−375.
[48] VALLETI K, PUNEET C, RAMA KRISHNA L, JOSHI S V. Studies on cathodic arc PVD grown TiCrN based erosion resistant thin films [J]. Journal of Vacuum Science & Technology A: Vacuum, Surfaces, and Films, 2016, 34: 041512.
[49] ALBERT SUE J, PERRY A J, VETTER J. Young's modulus and stress of CrN deposited by cathodic vacuum arc evaporation [J]. Surface and Coatings Technology, 1994, 68/69: 126−130.
[50] DATTA S, DAS M, BALLA V K, BODHAK S, MURUGESAN V K. Mechanical, wear, corrosion and biological properties of arc deposited titanium nitride coatings [J]. Surface and Coatings Technology, 2018, 344: 214−222.
[51] ASKARI E, FLORES P, DABIRRAHMANI D, APPLEYARD R. Study of the friction-induced vibration and contact mechanics of artificial hip joints [J]. Tribology International, 2014, 70: 1−10.
[52] VEGA J, SCHEERER H, ANDERSOHN G, OECHSNER M. Experimental studies of the effect of Ti interlayers on the corrosion resistance of TiN PVD coatings by using electrochemical methods [J]. Corrosion Science, 2018, 133: 240−250.
[53] SANKARA NARAYANAN T S N, KIM J, PARK H W. High performance corrosion and wear resistant Ti−6Al−4V alloy by the hybrid treatment method [J]. Applied Surface Science, 2020, 504: 144388.
[54] METIKOŠ-HUKOVIĆ M, KWOKAL A, PILJAC J. The influence of niobium and vanadium on passivity of titanium-based implants in physiological solution [J]. Biomaterials, 2003, 24: 3765–3775.
[55] ER D L, TAGHAVI POURIAN AZAR G, KAZMANLI K, ÜRGEN M. The corrosion protection ability of TiAlN coatings produced with CA-PVD under superimposed pulse bias [J]. Surface and Coatings Technology, 2018, 346: 1−8.
[56] CARRANZA R M, ALVAREZ M G. The effect of temperature on the passive film properties and pitting behavior of a Fe−Cr−Ni alloy [J]. Corrosion Science, 1996, 38: 909−925.
[57] CHUNG K H, LIU G T, DUH J G, WANG J H. Biocompatibility of a titanium–aluminum nitride film coating on a dental alloy [J]. Surface and Coatings Technology, 2004, 188/189: 745−749.
[58] AKHTAR S, MATIN A, MADHAN KUMAR A, IBRAHIM A, LAOUI T. Enhancement of anticorrosion property of 304 stainless steel using silane coatings [J]. Applied Surface Science, 2018, 440: 1286−1297.
[59] GOPI D, KARTHIKEYAN P, KAVITHA L, SURENDIRAN M. Development of poly (3, 4-ethylenedioxythiophene-co-indole-5-carboxylic acid) co-polymer coatings on passivated low-nickel stainless steel for enhanced corrosion resistance in the sulphuric acid medium [J]. Applied Surface Science, 2015, 357: 122−130.
[60] MADHANKUMAR A, NAGARAJAN S, RAJENDRAN N, NISHIMURA T. EIS evaluation of protective performance and surface characterization of epoxy coating with aluminum nanoparticles after wet and dry corrosion test [J]. Journal of Solid State Electrochemistry, 2012, 16: 2085−2093.

生物医用 Ti6Al4V 合金上电弧沉积 TiAlN 陶瓷涂层的表面、力学和体外腐蚀性能

Mohamed HUSSEIN[1], Madhan KUMAR[1], Nestor ANKAH[1,2], Ahmed ABDELAAL[2]

1. Interdisciplinary Research Center for Advanced Materials,
King Fahd University of Petroleum & Minerals, Dhahran 31261, Saudi Arabia;
2. Department of Mechanical Engineering, King Fahd University of Petroleum & Minerals,
Dhahran 31261, Saudi Arabia

摘　要：研究在医用 Ti6Al4V 合金上采用阴极电弧蒸发沉积制备的纳米晶 TiAlN 涂层的表面特性和体外腐蚀性能。采用 XRD 和 FE-SEM 对其结构和表面形貌进行分析，采用显微压痕法表征其表面的显微硬度，在模拟体液和人工唾液中进行体外腐蚀实验。结果表明：与无涂层合金相比，沉积 TiAlN 涂层后合金的表面硬度提高，为 44.4 GPa，弹性模量为 419.9 GPa，塑性变形能力增强，润湿角由(70.61±1.25)°增大到(86.27±2.2)°。生物腐蚀实验表明，沉积 TiAlN 涂层后，Ti6Al4V 合金的腐蚀电位显著正移约 150 mV，腐蚀电流密度显著降低约一个数量级，电荷转移电阻提高，证明合金的耐腐蚀性提高。与无涂层的合金相比，沉积 TiAlN 涂层后合金的表面性能、力学性能和耐腐蚀性能均有所提高。

关键词：CA-PVD；TiAlN；涂层；腐蚀；生物医用合金；钛

(Edited by Xiang-qun LI)